Polyhedron 131 (2017) 52–58

Contents lists available at ScienceDirect

Polyhedron

journal homepage: www.elsevier.com/locate/poly

Two Keggin polyoxometalate-based hybrid compounds with different helix: Syntheses, structure and catalytic activities

Peipei Zhu, Ning Sheng, Guodong Liu, Jingquan Sha *, Xiya Yang

Key Laboratory of Inorganic Chemistry in Universities of Shandong, Department of Chemistry and Chemical Engineering, Jining University, Qufu, Shandong 273155, China

ARTICLE INFO

Article history:
Received 4 March 2017
Accepted 18 April 2017
Available online 27 April 2017

Keywords:
Polyoxometalates
Hybrid
Helix
Catalyst
In Situ

ABSTRACT

By adjusting pH value, two new Keggin polyoxometalate-based hybrid compounds with different helical structure, $[Ag_6(btp)(pyttz)_6{\cdot}(HSiMo_{12}O_{40})_2]{\cdot}4H_2O$ (**1**) and $[Ag_2(pyttz)_4{\cdot}(H_2SiMo_{12}O_{40})_2]{\cdot}(TMA)_2{\cdot}4H_2O$ (**2**), (pyttz = 3-(pyrid-4-yl)-5-(1 H-1,2,4–3-yl)-1,2,4-triazolyl, btp = 5,5′-di(pyridin-4-yl)-1 H,1′H-3,3′-bi (1,2,4-triazole), TMA = tetramethylammonium), were successfully isolated by hydrothermal reaction and structurally characterized. Structural analysis shows the nature of the inorganic meso-helical channel in compound **1** and 2D homological helical layer in compound **2.** It is also interesting that a new organic ligand btp is formed in situ by the coupling of N-Heterocycle in **1**. In addition, the catalytic activities of **1** and **2** as solid-acid catalyst are explored, and the results indicate that **1** and **2** are a kind of highly-efficient and promising solid catalysts. Additionally, the proposed generation mechanism of btp in situ is also discussed.

1. Introduction

The design and synthesis of multifunctional, efficient and clean catalysts on industrial application is expected to have a major impact on industrial applications. Polyoxometalates (POMs) [1], as a family of well-defined metal-oxide clusters with attractive architecture and tunable properties, have been used as efficient catalyst to catalyze various chemical reactions due to their strong solid acidity, high efficient proton delivery, fast multi-electron transfer, and excellent reversible redox activity [2]. For example, POMs as Brønsted solid-acid catalysts can catalyze the oxidation of hydrocarbons [3], hydrolysis of ester [4], esterification of alcohols or carboxylic acid [5] and alkylation of aromatics [6]. And these has also been used as redox catalysts to degrade the organic dyes or toxic cation in waste water or toxic gas, such as, Rhodamine B (RhB) [7], methylene blue (MB) [8], methyl orange (MO) [9], 2-chlorophenol (2-CP) [10], azo group dyes[11], chromium ion (Cr^{6+}) [12], and so on. But the small surface areas (<10 $m^2\ g^{-1}$) and easily self-aggregation of the pure bulk POMs [13] limited their applications as solid catalysts. Thus, great efforts has been focused on loading POMs on different high-surface area supports, such as silica [14], activated carbon [15], molecular sieves [16], graphene or graphene oxide (GO) [17], coordination polymers [18] (CPs, including MOF [13,19]) and MHCs [20] (metal halide clusters)), and COFs [21] (covalent-organic frameworks)). Among the supports, POMs based coordination polymers (POMCPs) have been an important study field because of their well-defined and stable structures.

Since the compound with an inorganic double helix, $[(CH_3)_2NH_2]K_4[V_{10}O_{10}(H_2O)_2\text{-}(OH)_4(PO_4)_7].4H_2O$, was reported by Zubieta in Science [22], the assembly of POMCPs with helical structure have been attracted extensive research interests [23], because the kind of compounds have wide applications in the selective catalysis and optical devices as well [24]. In the work, two new POMCPs with different helix based on Keggin POMs and Ag-pyttz/btp or Ag-pyttz fragments have been synthesized through one-step hydrothermal reaction, formulated as $[Ag_6(btp)(pyttz)_6{\cdot}(HSiMo_{12}O_{40})_2]{\cdot}4H_2O$ (**1**) and $[Ag_2(pyttz)_4{\cdot}(H_2SiMo_{12}O_{40})_2]{\cdot}(TMA)_2{\cdot}4H_2O$, (pyttz = 3-(pyrid-4-yl)-5-(1H- 1, 2, 4–3-yl)-1,2,4-triazolyl, btp = 5,5′-di(pyridin-4-yl)-1H,1′H-3,3′-bi(1,2,4-triazole), TMA = tetramethylammonium). Note that a new organic ligand btp is generated in situ by the coupling of N-Heterocycle in **1**, and the proposed generation mechanism is discussed. In addition, by employing the esterification as reaction model, the catalytic activities of compounds **1** and **2** as solid–acid catalysts were also explored.

2. Experimental

2.1. Materials and general methods

The chemical materials were obtained commercially and used without further purification. The α-$H_4SiMo_{12}O_{40}$ clusters were

* Corresponding author.
E-mail address: shajq2002@126.com (J. Sha).

http://dx.doi.org/10.1016/j.poly.2017.04.017
0277-5387/

synthesized according to the reported literature [25]. The Elemental analyses of the C, H and N were measured by the Perkin–Elmer 2400 CHN elemental analyzer. Infrared Spectrum (IR) was obtained from the Alpha Centaurt FT/IR spectrometer with KBr pellets. The XRD pattern was scanned by the Rigaku D/MAX 2500 V XRD diffractometer with Cu Kα radiation. The diffuse reflectance spectra were scanned on T9 spectrometer, and the UV−Vis spectra were recorded on a 756 CRT spectrophotometer.

2.2. Synthesis of $[Ag_6(btp)(pyttz)_6{\cdot}(HSiMo_{12}O_{40})_2]{\cdot}4H_2O$ (1)

α-$H_4[SiMo_{12}O_{40}]$, (300 mg, 0.16 mmol), $AgNO_3$ (150 mg, 0.88 mmol), pyttz ligand (80 mg, 0.54 mmol), tetramethylammonium hydroxide (TMAH) (0.20 mmol) were dissolved in distilled water (10 mL) with stirring for 2 h at room temperature, and pH value was adjusted to *ca.* 2.16 by 1 mol L^{-1} HCl. The resulting solution was transferred and sealed in a 20 mL Teflon-lined stainless steel reactor and heated at 170 °C for 5 days. After the autoclave was cooled to room temperature at 10 °C h^{-1}, the blue block crystal suitable for X-ray crystallography were obtained, and then washed with distilled water and air-dried (yield: 32% based on Ag). Elemental analysis: *Anal.* Calcd for $C_{68}H_{62}Ag_6Si_2Mo_{24}N_{50}O_{84}$ (5929.6): C 13.77, H 1.05 and N 11.81%; Found C 13.64; H 1.23 and N 11.78%. IR (KBr pellet, cm^{-1}): 3497 (w), 3105 (w), 1641 (s), 951 (s), 904 (s), 791 (s), 628 (w), 623 (w), 508 (w).

2.3. Synthesis of $[Ag_2(pyttz)_4{\cdot}(H_2SiMo_{12}O_{40})_2]{\cdot}(TMA)_2{\cdot}4H_2O$ (2)

The preparation of **2** was similar to that of compound **1**, except that the pH values was adjusted 3.54. The light yellow block crystal of **2** (yield: 43% based on Ag) was successfully isolated. Elemental analysis: *Anal.* Calcd for $C_{44}H_{64}Ag_2Si_2Mo_{24}N_{30}O_{84}$ (4931.7): C 10.72, H 1.31 and N 8.52%; Found C 10.57; H 1.46 and N 8.46%. IR (KBr pellet, cm^{-1}): 3312 (w), 3231 (w), 1640 (s), 1482 (s), 1234 (s), 956 (s), 906 (s), 795 (s), 631 (w), 505 (w).

2.4. Catalytic synthesis of acetylsalicylic acid

Salicylic acid (1.5 g, 10.86 mmol) was transferred to a clean, dry three-necked flask with the volume of 50 mL. The acetic anhydride (3.0 mL) and compounds (40 mg, 0.0067 mmol for **1** or 0.0081 mmol for **2**) were dispersed in the three-necked flask, respectively. The reaction was carried out in water bath (75–90 °C) for 60 min. At 5, 10, 15, 20, 25, 30, 35, 40, 45, 50, 55 and 60 min, the sample (10 μL) was taken out from the flask and diluted with PBS buffer solution for UV–Vis analysis. According to ultraviolet two-wavelength isoabsorption spectrophotometry ($A = A_1 + A_2$), the content of salicylic acid (SA) and acetylsalicylic Acid (ASP) were detected, which the high reliability, accuracy of the detection technology had been proved (ESI† and Eqs. (1) and (2).

$$C_{SA} = 39.8586A297 - 1.5328A_{270} - 0.7647 \quad (1)$$

$$C_{ASP} = 387.7989A_{270} - 87.7713A_{297} - 6.5271 \quad (2)$$

2.5. X-ray Crystallographic measurements

Crystallographic data for compounds were collected on the Agilent Technology Eos Dual system with Mo Kα radiation (λ = 0.71069 Å) at room temperature. The structure of compounds was solved by the direct method and refined full-matrix last squares on F^2 through the SHELXTL and WINGX software package [26]. All non-hydrogen atoms were refined anostropically and the ISOR, DELU and SIMU command was used to refine some APD and NPD atoms the bond length between some atoms in **1** and **2**. The crystal data and selected bond lengths and angles are listed in Table 1 and Table S12. The CCDC reference number of compounds **1** and **2** is 1495425 and 1495426.

3. Results and discussion

Single-crystal X-ray diffraction analysis shows that the supramolecular frameworks of compounds **1** and **2** exhibit the different helical structure. According to the bond valence sum calculation [27], $S = \sum\exp[-(R - R_o)/B]$ (S = bond valence, R = bond length), all Mo atoms are in the full oxidation state. To balance the charge, the protons are added and compounds are formulated as $[Ag_6(btp)(pyttz)_6{\cdot}(HSiMo_{12}O_{40})_2]{\cdot}4H_2O$ for **1** and $[Ag_2(pyttz)_4{\cdot}(H_2SiMo_{12}O_{40})_2]{\cdot}(TMA)_2{\cdot}4H_2O$ for **2**. The parallel experiments have indicated that the use of TMAH species was necessary for the isolation of the compounds **1** and **2**, although it was not involved in the final structures in **1**. If not, compounds 1 and 2 cannot be isolated.

3.1. Structure and Topological analysis of compound 1

Compound **1** is consisted of two $[SiMo_{12}O_{40}]^{4-}$ clusters (abbr. $SiMo_{12}$), six Ag^+ ions, six pyttz ligands, one btp ligand and four water molecules in Fig. S1 (supporting information). There are three crystallography independent Ag^+ ions (Ag1, Ag2 and Ag3) with three kinds of coordination modes in Fig. S2 (supporting information): Ag1 exhibits screwy pyramidal geometry coordinated with four N atoms from two pyttz ligands and one O atom from the $SiMo_{12}$ clusters; Ag2 adopts triangular pyramid geometry completed by three N atoms from one pyttz ligand and one btp ligand and one O atom from the $SiMo_{12}$ clusters; Ag3 shows triangle geometry completed by three N atoms from two pyttz ligands. In turn, the $SiMo_{12}$ clusters as two-connected inorganic ligands

Table 1
Crystallographic and structural refinement data for **1** and **2**.

Compound	Compound **1**	Compound **2**
Chemical formula	$C_{68}H_{62}Ag_6Si_2Mo_{24}N_{50}O_{84}$	$C_{44}H_{64}Ag_2Si_2Mo_{24}N_{30}O_{84}$
CCDC no.	1495425	1495426
Formula weight	5929.6	4931.7
Temperature (K)	293(2)	293(2)
Wavelength (Å)	0.71069	0.71069
Crystal system	triclinic	triclinic
Space group	$P\bar{1}$	$P\bar{1}$
a (Å)	12.174(5)	11.7027(3)
b (Å)	12.766(5)	13.3019(6)
c (Å)	23.329(5)	19.2198(6)
α (°)	93.590(5)	92.951(3)
β (°)	90.790(5)	99.439(2)
γ (°)	110.640(5)	93.295(3)
V (Å^3)	3384(2)	2940.88(18)
Z	1	1
ρ (g cm^{-3})	3.124	2.782
μ (mm^{-1})	5.646	5.808
$F(000)$	2804.0	2336.0
θ (°)	3.235–25.000	3.41–25.000
Reflections collected	16491	22404
Independent reflections (R_{int})	11904 (0.0234)	10333 (0.0267)
Data/restraints/parameters	11904/33/1054	10333/43/877
Goodness-of-fit on F^2	1.061	1.093
Final R indices [$I > 2\sigma(I)$]	R_1 = 0.0426, wR_2 = 0.0938	R_1 = 0.0667, wR_2 = 0.1822
R indices (all data)	R_1 = 0.0568, wR_2 = 0.1014	R_1 = 0.0846, wR_2 = 0.2077
Largest diff. peak and hole (e Å^{-3})	3.136 and −1.434	2.756 and −2.274

[a] $R_1 = \sum||F_o| - |Fc||/\sum|F_o|$. [b] $wR_2 = \{\sum[w(F_o^2 - F_c^2)^2]/\sum[w(F_o^2)^2]\}^{1/2}$.

coordinate with two Ag cations (Ag1 and Ag2). And all bond lengths and angles around Ag ions are within the normal ranges, which are in range of 2.519–2.623 Å for Ag–O bonds, 2.129–2.791 Å for Ag–N bonds and 71.0–168.3° for N–Ag–N angles.

In compound **1**, six Ag^+ ions (two Ag1, two Ag2 and two Ag3) with six pyttz and one btp fabricate one $[Ag_6(btp)(pyttz)_6]^{6+}$ subunit. Then the adjacent subunits link with each other to form a 2D supramolecular net *via* the non-covalent interaction (2.128 Å for N_{11}–H_{20}–N_{20}, 2.713 Å for N_{24}–H_{24}–C_{24}, 2.392 Å for N_{10}–H_{17}–C_{17} and 2.628 Å for N_{17}–H_8–C_8) in Fig. 1a. Finally, Ag1 and Ag2 ions in the 2D nets coordinate with oxygen atoms of the SiM_{O12} clusters to construct the 3D frameworks in Fig. 1b. To better comprehend the structure, the 3D structure can be rationalized as a (2, 4, 5) connecting network with {6} $\{4^2.6^3.8\}\{4^2.6^5.8^3\}$ topology. In this simplification, the 2-connected nodes are $SiMo_{12}$ clusters, and 4-connected nodes Ag1 and 5-connected nodes Ag2. It is interesting that there is one kind of helical channel constructed by the left- and right-handed helical chains. More specifically, the sphere $SiMo_{12}$ clusters as V-shaped inorganic ligands link with Ag1 and Ag2 ions fabricating the helical chains with a pitch of screw (12.174 Å) along *a* axis *via* the route of –$SiMo_{12}$–Ag_2–$SiMo_{12}$–Ag_1–Ag_2–Ag_2–$SiMo_{12}$– for left-handed helix and –$SiMo_{12}$–Ag_2–Ag1–$SiMo_{12}$–Ag_2–Ag_2–$SiMo_{12}$– for right-handed helix. And pitches of screw are consistent with the unit length of *a* axis (12.174 Å). Furthermore, two kinds of helical chains with different orientations are perfectly enclosed by sharing [Ag_1–$SiMo_{12}$–Ag_2] framework forming a 1D channel shown in Fig. 1c.

3.2. Structure and Topological analysis of compound 2

Compound **2** is consisted of two $SiMo_{12}$ clusters, two Ag cations, four pyttz ligands, two $[TMA]^+$ ions and four water molecules in Fig. S3 (supporting information). There is one crystallography independent Ag cation (Ag1) and two crystallography independent $SiMo_{12}$ clusters (named Si-I and Si-II) in Fig. S4 (supporting information): Ag1 ion is coordinated by four N atoms from two pyttz ligands and two O atoms from Si-I clusters; in turn, Si-I clusters as two-connected inorganic ligands coordinate with two Ag1 ions. And all bond lengths and angles around Ag ions are within the normal ranges, which are in range of 3.07–3.08 Å for Ag–O bonds, 2.406–2.500 Å for Ag–N bonds and 70.6–162.5° for N–Ag–N angles.

In compound **2**, the Si-I clusters coordinate with two $[Ag(pyttz)_2]^+$ subunits forming the "Ag–Si-I–Ag" molecular fragment, then the molecular fragments connect with each other constructing a "ripple-shaped" chain *via* non-covalent interaction (2.713 Å for N_6–H_6–H_6–N_6) in Fig. 2a. Finally, many interlaced 1D "ripple-shaped" chains are assembled together by Si-II clusters fabricating the 3D supramolecular hybrid frameworks with $\{3^2.4^2.5^2\}\{3^2.4^3.5^4.6^3.7^2.8\}\{6\}$ topology, in which the Si-II clusters as a four-connected nodes link with four pyttz molecular through intermolecular interaction (2.579 Å for O_{25}–H_{14}–C_{14}, 2.388 Å for O_{14}–H_{10}–C_{10} and 2.517 Å for O_{21}–H_{10}–C_{10}) in Fig. 2b. Interesting is that there are also left- and right-handed helical chains with the same pitch of screw (13.30 Å) along the *b* axis in the 3D frameworks, which are constructed *via* the route of –Si(I)–Ag1–Ag1–Si(II)–Ag1–Si(I)– for the left-handed helix and –Si(I)–Ag1–Si(II)–Ag1–Ag1–Si(I)– for the right-handed helix. Different from the helix of **1**, the identical left- or right-handed helical chains are fused together in a hand-by-hand mode *via* Ag1 generating 2D homological helical layer with 1D channel. Finally, the different 2D homological helical layers are connected together forming 3D framework through sharing with the Si-II clusters in Fig. 2c.

3.3. Generation mechanism of btp ligand in situ

Many parameters, such as temperature, pH values, time, and the type and molar ration of reactants, can affect the final structure of the compounds in hydrothermal reactions. Compared with the

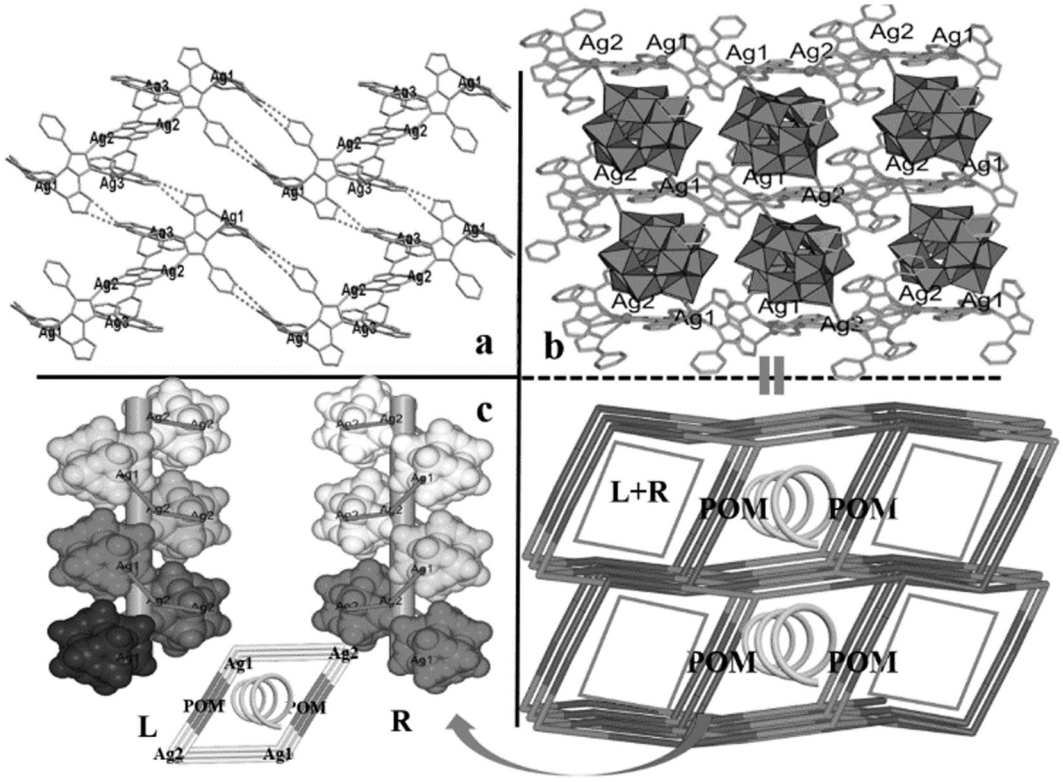

Fig. 1. (a) Representation of the 2D nets constructed by $[Ag_6(btp)(pyttz)_6]^{6+}$ subunit *via* the hydrogen bond. (b) Combined ball/stick/polyhedron and topology representation of 3D inorganic–organic hybrid frameworks constructed by the 2D nets and SiM_{O12} clusters. (c) Combined stick/space filled representation of the left- and right-handed helical chains completed by $SiMo_{12}$ clusters with Ag1 and Ag2 ions.

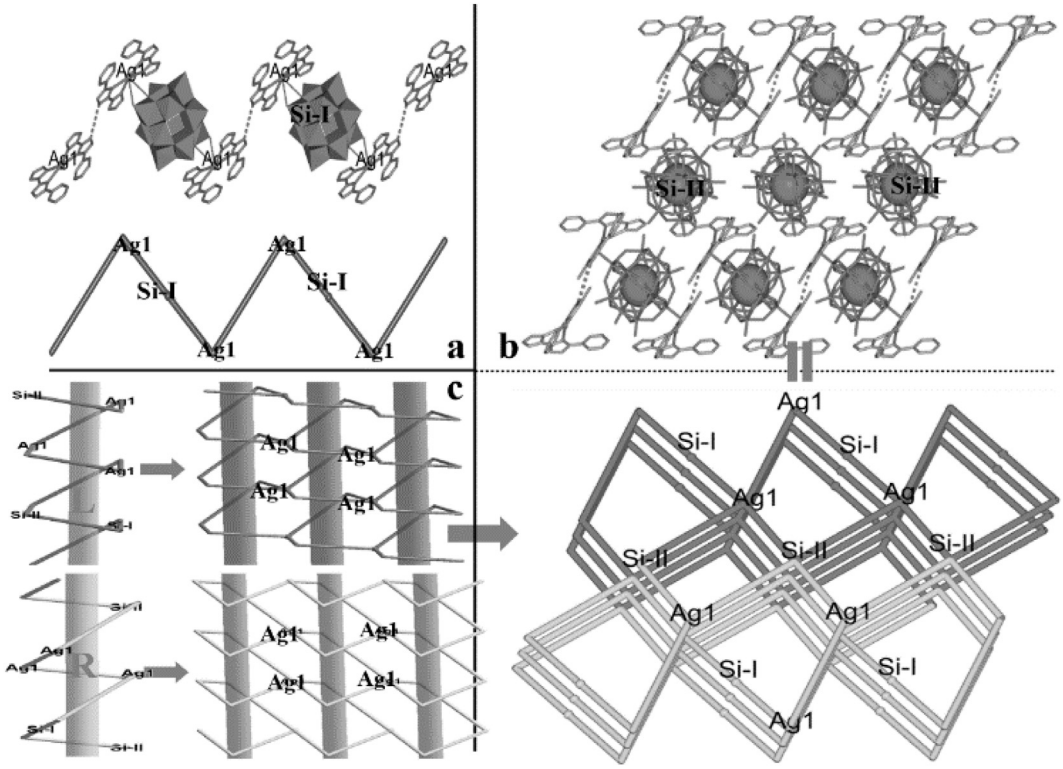

Fig. 2. (a) Combined ball/stick representation of the 1D "ripple-shaped" chain formed by Ag1–Si(I)–Ag1″ molecular fragment *via* hydrogen bonds. (b) Combined ball/stick and topology representation of 3D supramolecular hybrid frameworks constructed by the interlaced 1D "ripple-shaped" chains and Si-II clusters. (c) Topology representation of 2D homological helical layer with 1D channel constructed by $SiMo_{12}$ clusters (Si-I and Si-II) and Ag1 and Ag2 ions *via* the route of –Si(I)–Ag1–Ag1–Si(II)–Ag1–Si(I)– for the left-handed helix and –Si(I)–Ag1–Si(II)–Ag1–Ag1–Si(I)– for the right- handed helix.

structures and synthesis condition of **1** and **2** and $[Ag_{10}(pyttz)_6(trz)_2(H_2O)_6]$ $[HP_2W_{18}O_{62}]_2{\cdot}8H_2O$ [18]a shown in table 2, we can speculate that POMs and pH values synergistically induce the formation of btp molecules, and the generation mechanism is proposed in scheme 1. First, thanks to the inductive effect of Ag ions, the coordination between the pyridine of triazole and Ag ions can reduce the electron cloud density and stability of C–C bond between two triazole cycles. Meanwhile, the protonated pyridine and triazole can also attract the electron of the C–C bond between two triazole rings and reduce the electron cloud density, which is a key factor for the generation of btp molecular. Additionally, the chemical bonds of the pyttz molecules occurred violent vibration under the hydrothermal conditions. As a result, C–C bonds between two triazole rings can generate heterolytic cleavage reaction to form intermediates (B) with negative charge, which similar to the case of $[Ag_{10}(pyttz)_6(trz)_2(H_2O)_6]$ $[HP_2W_{18}O_{62}]_2{\cdot}8H_2O$ [18]a. Because of the pseudo-liquid phase catalytic behaviour and excellent redox of POMs, a series of electron transfer among $SiMo_{12}$ clusters and intermediates B may result that some intermediates B is converted into the intermediates C with positive electricity.

Table 2
In situ synthesis of new ligand from pyttz ligand in different pH values in POMs system.

Molecular Formula	pH	$[Ag_mL_n]^{m+}$	In Situ
$[Ag_6(btp)(pyttz)_6{\cdot}(HSiMo_{12}O_{40})_2]{\cdot}4H_2O$	2.16	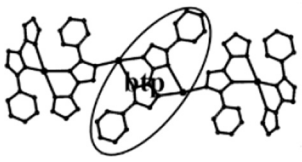	Yes
$[Ag_{10}(pyttz)_6(trz)_2{\cdot}(H_2O)_6]$ $[HP_2W_{18}O_{62}]_2{\cdot}8H_2O$	2.0	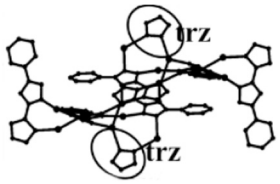	Yes
$[Ag_2(pyttz)_4{\cdot}(H_2SiMo_{12}O_{40})_2]{\cdot}(TMA)_2{\cdot}4H_2O$	3.54	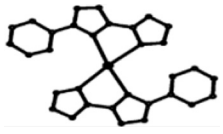	No

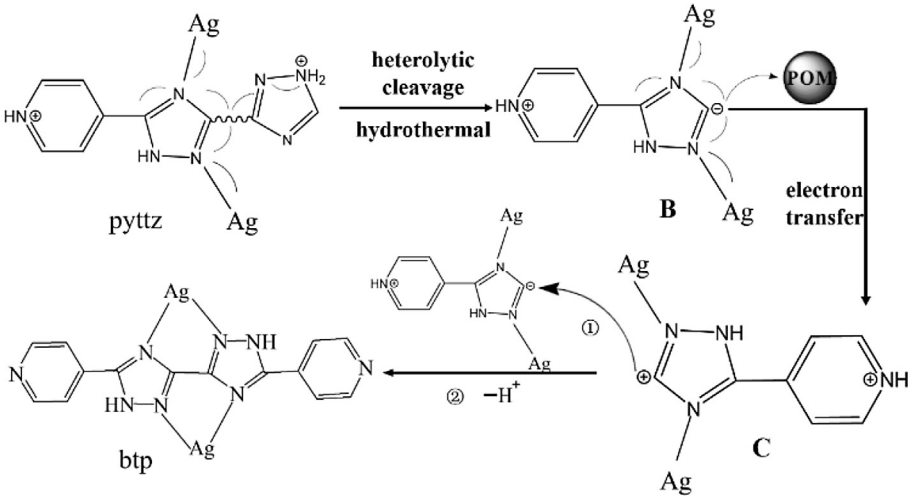

Scheme 1. The proposed mechanism of the generation of btp from pyttz in POM system.

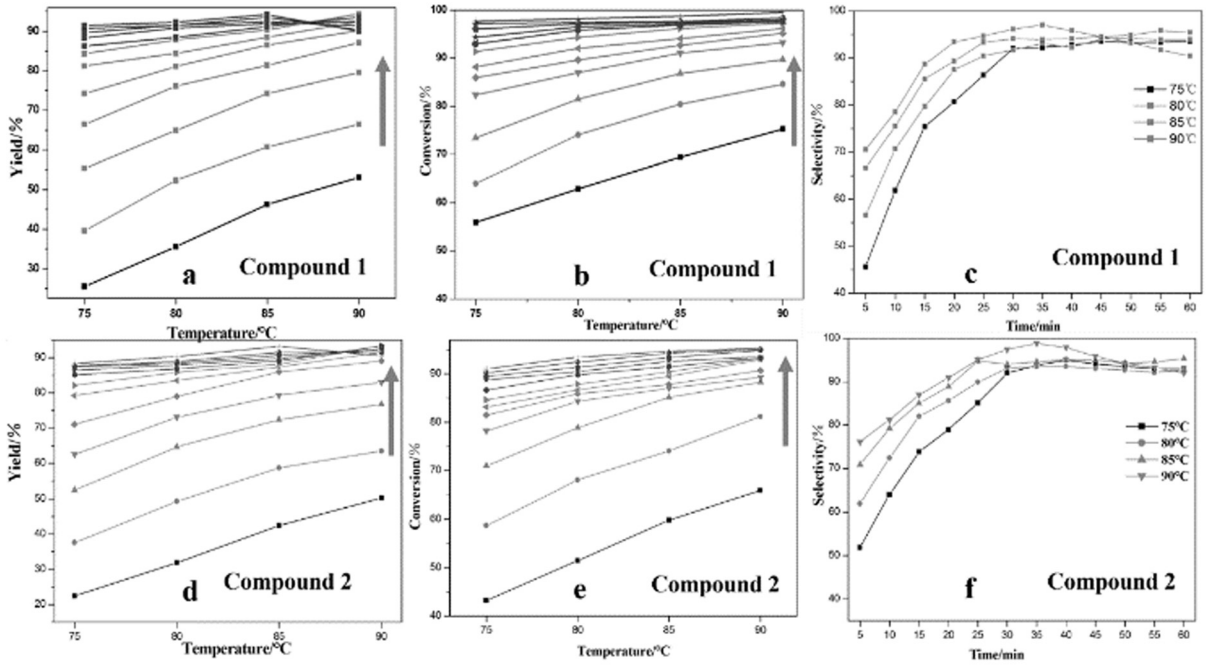

Fig. 3. Catalytic activity of compounds **1** and **2** as solid–acid catalyst: (a/d) Yield of acetylsalicylic acid *vs* the reaction temperature; (b/e) Conversion rate of salicylic acid *vs* the reaction temperature (75–90 °C), and (c/f) the selectivity of catalysts *vs* the reaction time (5–60 min).

Finally, intermediates B and C with opposite charge combine together to form the new btp molecules *via* electrostatic interaction.

3.4. IR Spectrum, XRD pattern and Electronics absorption spectra

IR spectra of compounds **1** and **2** before and after the catalytic experiment are presented in Fig. S5 (supporting information). The characteristic peak at 904, 951, and 791 cm^{-1} for **1**, 906, 956, and 794 cm^{-1} for **2** are attributed to *v* (Si–O), *v* (Mo═O), and *v* (Mo–O–Mo) vibrations, respectively. Bands in the regions of 1641–1091 cm^{-1} for **1**, 1640–1094 for **2** are attributed to the pyttz and btp organic ligand. And the XRD patterns are shown in Fig. S6 (supporting information). The peak position of simulation and experiment patterns match well expect for reflection intensities, which confirms the higher purity of compounds. In addition, the electronic absorption spectra of **1** and **2** were recorded in the crystalline state at room temperature, Fig. S7 (supporting information), shows strong absorption bands in the range from 200 to 800 nm. Obviously, the absorption is broadened and strengthened by the overlap of the bands of O–Ag, O–Mo, and the Ag-pyttz/btp fragments.

3.5. Esterification properties

As we all know, the synthesis of acetylsalicylic acid is an acid-catalyzed reaction. To investigate the catalytic activities of **1** and **2** as solid–acid catalysts, the catalytic synthesis of acetylsalicylic acid as model reaction was carried out under different reaction time (5, 10, 15, 20, 25, 30, 35, 40, 45, 50, 55 and 60 min) and temperature (75, 80, 85 and 90 °C), which are evaluated through the yield of acetylsalicylic acid, the conversion rate of salicylic acid

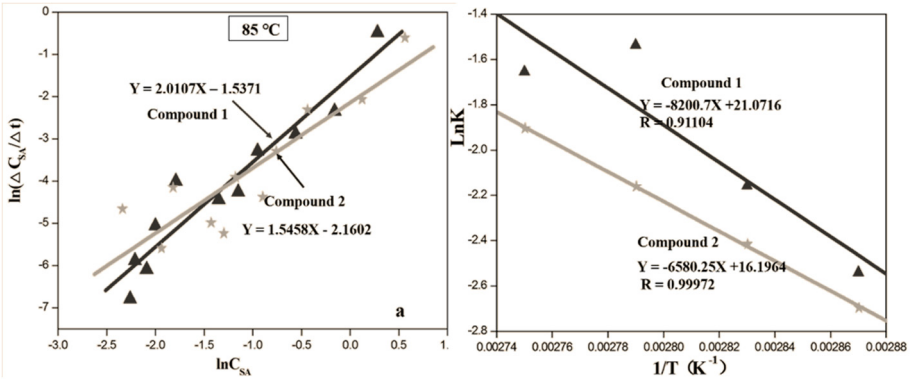

Fig. 4. (a) The linear relationship of $\ln(\Delta C_{SA}/\Delta t)$ with $\ln C_{SA}$ for compounds **1** and **2** at 358 K. (b) The linear relation of $\ln k$ with T^{-1} at 348 K, 353 K, 358 K and 363 K.

and the selectivity of catalysts. As is shown in Fig. 3 and Tables S1–10 (supporting information), keeping the same reaction time, the higher the reaction temperature is, the higher the conversion rate of salicylic acid is, and so are the yield of acetylsalicylic acid and the selectivity of catalysts. Note that the increasing trend of three physical quantities changes slowly with the temperature rising after 35 min. In turn, three physical quantities are significantly enlarged with increasing the time during the initial period of 5–40 min under the same temperature. When the reaction temperature is higher than 90 °C, three physical quantities changes in an irregular manner, which may be due to the occurrence of the side effects. Taking into account the cost as well as the energy and efficiency, the reaction time 35 min and the temperature 85 °C were employed in the work, and the yield of acetylsalicylic acid is 90.3% for **1** and 88.12% for **2**, and the conversion rate of salicylic acid 96.16% for **1** and 93.14% for **2**, and the selectivity of catalyst of 93.91% for **1** and 94.61% for **2**. Compared with other catalyst, **1** and **2** as solid–acid catalyst exhibit roughly the same catalytical activities as H_2SO_4 (85%) [28] and POM/ZrO_2 (94.2%) [29]. However, **1** and **2** could be readily isolated from the reaction mixture by simple filtration, and then the results of the following subsequent run shows that the catalytic activities little fall Fig. S8 (supporting information). Above results indicate that compounds **1** and **2** possess high activity and stability, and are a green and environmentally benign catalyst.

To quantitatively evaluate the reaction kinetics for the esterification by the utilization of **1** and **2** as catalyst, the reaction rate equation model is set up to obtain the rate constant (κ) and reaction order (n):

$$r_{SA} = dC_{SA}/dt = \kappa C_{SA}^{n} \quad (3)$$

$$\ln(dC_{SA}/dt) = \ln\kappa + n\ln C_{SA} \quad (4)$$

According to Eq. (4) and Fig. 4a, the κ and n values at 358 K are 0.215 and 2.0107 for **1** and 0.1154 and 1.5458 for **2**, respectively. And the correlation coefficient (R) shows good statistics values. Then the rate equations of **1** and **2** are obtained as following:

$$r_{SA} = 0.215\ C_{SA}^{2.0107} \quad (5)$$

$$r_{SA} = 0.1154\ C_{SA}^{1.5458} \quad (6)$$

In a same way, the κ values at 348 K, 353 K and 363 K are obtained as 0.0788, 0.1156 and 0.1256 of **1**, and 0.0674, 0.0893 and 0.1489 of **2**, respectively (Fig. 4b and Table S11 (supporting information).

4. Conclusions

In summary, two new POMCPs with different helical structure were successfully synthesized under different pH value and the assistance of TMA. Note that a new organic ligand btp is generated in situ in **1**, and generation mechanism indicates that POMs and pH values synergistically induce the formation of btp molecules under the mild acid condition. In addition, the yield of acetylsalicylic acid by employing **1** and **2** as acid catalysts is 90.3% for **1** and 88.12% for **2**, which are similar to that reported in the literature. However, **1** and **2** could be readily isolated from the reaction mixture by simple filtration and reuse several times. The results indicate that **1** and **2** as heterogeneous catalyst possess high activity and stability, and are a green and environmentally benign catalyst.

Acknowledgements

This work is financially supported by the National Natural Science Foundation of China (Grant No. 21271089), and Talent Culturing Team Plan for Leading Disciplines of University in Shandong Province, China Postdoctoral Science Foundation (2016M600914) and the training program for New Century Excellent Talents in universities (1253-NCET-022).

Appendix A. Supplementary data

CCDC (1495425 and 1495426) contains the supplementary crystallographic data for compounds **1** and **2**. These data can be obtained free of charge *via* http://dx.doi.org/10.1016/j.poly.2017.04.017, or from the Cambridge Crystallographic Data Centre, 12 Union Road, Cambridge CB2 1EZ, UK; fax: (+44) 1223-336-033; or e-mail: deposit@ccdc.cam.ac.uk. Tables of selected bond lengths (Å), bond angles (deg) and concentration and conversation of salicylic acid (SA), acetyl salicylic acid (ASP) under different temperature and different time. The standard curve equation of salicylic acid and acetyl salicylic acid and IR, XRPD and the diffuse reflectance spectrum and structural figures for the compounds **1** and **2** are provided in supporting information.

Supplementary data associated with this article can be found, in the online version, at http://dx.doi.org/10.1016/j.poly.2017.04.017.

References

[1] (a) N. Li, B. Mu, L. Lv, R.D. Huang, J. Solid State Chem. 226 (2015) 88;
(b) C.J. Zhang, H.J. Pang, M.X. Hu, J. Li, Y.G. Chen, J. Solid State Chem. 182 (2009) 1772;
(c) Y.N. Chi, F.Y. Cui, Z.G. Lin, Y. Xu, X.Y. Ma, P.P. Shen, K.L. Huang, C.W. Hu, J. Solid State Chem. 199 (2013) 230;
(d) H.J. Pang, M. Yang, L. Kang, H.Y. Ma, B. Liu, S.B. Li, H. Liu, J. Solid State Chem. 198 (2013) 440;

(e) D.L. Long, C. Streb, Y.F. Song, S. Mitchell, L. Cronin, J. Am. Chem. Soc. 130 (2008) 1830;
(f) D.L. Long, R. Tsunashima, L. Cronin, Angew. Chem., Int. Ed. 49 (2010) 1736.
[2] (a) T. Yamase, Chem. Rev. 98 (1998) 307;
(b) S.T. Zheng, G.Y. Yang, Chem. Soc. Rev. 41 (2012) 7623;
(c) Y.F. Song, R. Tsunashima, Chem. Soc. Rev. 41 (2012) 7384;
(d) J. Miao, Y.W. Liu, Q. Tang, D.F. He, G.C. Yang, Z. Shi, S.X. Liu, Q.Y. Wu, Dalton Trans. 43 (2014) 14749;
(e) H. Lv, Y.V. Geletii, C. Zhao, J.W. Vickers, G. Zhu, Z. Luo, J. Song, T. Lian, D.G. Musaev, G.L. Hill, Chem. Soc. Rev. 41 (2012) 7572;
(f) S.S. Wang, G.Y. Yang, Chem. Rev. 115 (2015) 4893.
[3] (a) Q.X. Han, C. He, M. Zhao, B. Qi, J.Y. Niu, C.Y. Duan, J. Am. Chem. Soc. 135 (2013) 10186;
(b) O.A. Kholdeeva, N.V. Maksimchuk, G.M. Maksimov, Catal. Today 157 (2010) 107;
(c) W. Adam, P.L. Alsters, R. Neumann, C.R. Saha-Möller, D. Seebach, R. Zhang, Org. Lett. 5 (2003) 725.
[4] D.B. Dang, Y. Bai, C. He, J. Wang, C.Y. Duan, J.Y. Niu, Inorg. Chem. 49 (2010) 1280.
[5] (a) H. Miao, G.H. Hu, J.Y. Guo, H.X. Wan, H. Mei, Y. Zhang, Y. Xu, Dalton Trans. 44 (2015) 694;
(b) G.H. Hu, H. Miao, H. Mei, S. Zhou, Y. Xu, Dalton Trans. 45 (2016) 7947.
[6] A. Corma, S. Iborra, F.X. Llabrés, I. Xamena, R. Montón, J.J. Calvino, C. Prestipino, J. Phys. Chem. C. 14 (2010) 8828–8836.
[7] (a) H.P. Zhen, X.L. Li, L.J. Zhang, H. Lei, C. Yu, Y.S. Zhou, S. Hassan, L.B. Qin, H.M. Asif, RSC Adv. 5 (2015) 24550;
(b) K. Wang, D.D. Zhang, J.C. Ma, P.T. Ma, J.Y. Niu, J.P. Wang, CrystEngComm 14 (2012) 3205;
(c) Y.Y. Hu, X. Zhang, D.C. Zhao, H.Y. Guo, L.W. Fu, L.L. Guo, X.B. Cui, Q.S. Huo, J. Q. Xu, Dalton Trans. 44 (2015) 14830.
[8] (a) L.J. Xu, W.Z. Zhou, L.Y. Zhang, B. Li, H.Y. Zang, Y.H. Wang, Y.G. Li, CrystEngComm 17 (2015) 3708;
(b) Y.F. Zhao, Y.Y. Yuan, X. Du, X.H. Lin, F.H. Liao, J.L. Xie, J.H. Lin, J.L. Sun, CrystEngComm 18 (2016) 521;
(c) Z.J. Liu, S. Yao, Z.M. Zhang, E.B. Wang, RSC Adv. 3 (2013) 20829.
[9] (a) X.L. Wang, N. Li, A.X. Tian, J. Ying, T.J. Li, X.L. Lin, J. Luan, Y. Yang, Inorg. Chem. 53 (2014) 7118;
(b) Y.Q. Chen, G.R. Li, Y.K. Qu, Y.H. Zhang, K.H. He, Q. Gao, X.H. Bu, Cryst. Growth Des. 13 (2013) 901;
(c) X.J. Dui, W.B. Yang, X.Y. Wu, X.F. Kuang, J.Z. Liao, R.M. Yu, C.Z. Lu, Dalton Trans. 44 (2015) 9496.
[10] J. Li, J. Yang, Y.Y. Liu, J.F. Ma, Chem. Eur. J. 21 (2015) 1.
[11] A. Dolbecq, P. Mialane, B. Keita, L. Nadjo, J. Mater. Chem. 22 (2012) 24509.
[12] X.L. He, Y.P. Liu, K.N. Gong, Z.G. Han, X.L. Zhai, Inorg. Chem. 4 (2015) 1215.
[13] C.Y. Sun, S.X. Liu, D.D. Liang, K.Z. Shao, Y.H. Ren, Z.M. Su, J. Am. Chem. Soc. 131 (2009) 1883.
[14] (a) G. Peng, Y.H. Wang, C.W. Hu, E.B. Wang, S.H. Feng, Y.C. Zhou, H. Ding, Y.Y. Liu, Appl. Catal., A. 218 (2001) 91;
(b) Y. Guo, Y. Wang, C. Hu, Y. Wang, E. Wang, Y. Zhou, S. Feng, Chem. Mater. 12 (2000) 3501;
(c) Y. Guo, C.J. Hu, Mol. Catal. A. 262 (2007) 136.
[15] (a) R.D. Gall, C.L. Hill, J.E. Walker, Chem. Mater. 8 (1996) 2523;
(b) B.A. Watson, M.A. Barteau, L. Haggerty, A.M. Lenhoff, R.S. Weber, Langmuir 8 (1992) 1145.
[16] (a) C.T. Kresge, M.E. Leonowicz, W.J. Roth, J.C. Vartuli, J.S. Beck, Nature 359 (1992) 710;
(b) D. Zhao, J. Feng, Q. Huo, N. Melosh, G.H. Fredrickson, B.F. Chmelka, G.D. Stucky, Science 279 (1998) 548.
[17] (a) S. Wang, H.L. Li, L.Y. Zhang, B. Li, X. Cao, G.H. Zhang, S.L. Zhang, L.X. Wu, Chem. Commun. 50 (2014) 9700;
(b) H.L. Li, S.P. Pang, X.L. Feng, K. Müllen, C. Bubeck, Chem. Commun. 46 (2010) 6243;
(c) Y.Y. Chen, M. Han, Y.Y. Tang, J.C. Bao, S.L. Li, Y.Q. Lan, Z.H. Dai, Chem. Commun. 51 (2015) 12377;
(d) S.Z. Wen, W. Guan, J.P. Wang, Z.L. Lang, L.K. Yan, Z.M. Su, Dalton Trans. 41 (2012) 4602.
[18] (a) P.P. Zhu, L.J. Sun, N. Sheng, J.Q. Sha, G.D. Liu, L. Yu, H.B. Qiu, S.X. Li, Cryst. Growth Des. 16 (2016) 3215;
(b) L. Li, J.W. Sun, J.Q. Sha, G.M. Li, P.F. Yan, C. Wang, L. Yu, Dalton Trans. 44 (2015) 1948;
(c) J.Q. Sha, P.P. Zhu, X.Y. Yang, N. Sheng, J.S. Li, L.J. Sun, H. Yan, CrystEngComm 18 (2016) 7049;
(d) Q. Sha, J.L.J. Sun, P.P. Zhu, J.Z. Jiang, CrystEngComm 18 (2016) 283.
[19] (a) B. Nohra, H.E. Moll, L.M.R. Albelo, P. Mialane, J. Marrot, C.M. Draznieks, M. O'Keeffe, R.N. Biboum, J. Lemaire, B. Keita, L. Nadjo, A. Dolbecq, J. Am. Chem. Soc. 133 (2011) 13363;
(b) L.M.R. Albelo, A.R.R. Salvador, A. Sampieri, D.W. Lewis, A. Gómez, B. Nohra, P. Mialane, J. Marrot, F. Sécheresse, C.M. Draznieks, R.N. Biboum, B. Keita, L. Nadjo, A. Dolbecq, J. Am. Chem. Soc. 131 (2009) 16078;
(c) A. Dolbecq, P. Mialane, F. Sécheresse, B. Keita, L. Nadjo, Chem. Commun. 48 (2012) 8299;
(d) D.Y. Shi, C. He, W.L. Sun, Z. Ming, C.G. Meng, C.Y. Duan, Chem. Commun. 52 (2016) 4714.
[20] (a) L.N. Xiao, Y.Y. Hu, L.M. Wang, Y. Wang, J.N. Xu, H. Ding, X.B. Cui, J.Q. Xu, CrystEngComm 14 (2012) 8589;
(b) J.P. Wang, P.T. Ma, J.Y. Niu, Inorg. Chem. Commun. 9 (2006) 1049;
(c) S.Z. Li, P.T. Ma, H.Z. Niu, J.W. Zhao, J.Y. Niu, Inorg. Chem. Commun. 13 (2010) 805;
(d) X.L. Wang, C. Qin, E.B. Wang, Z.M. Su, Y.G. Li, L. Xu, Angew. Chem., Int. Ed. 44 (2005) 5824.
[21] (a) H.P. Ma, B.L. Liu, B. Li, L.M. Zhang, Y.G. Li, H.Q. Tan, H.Y. Zang, G.S. Zhu, J. Am. Chem. Soc. 138 (2016) 5897;
(b) M.P. Santoni, A.K. Pal, G.S. Hanan, A. Proust, B. Hasenknopf, Inorg. Chem. 50 (2011) 6737;
(c) H.F. Gao, H.F. Cheng, Z.H. Yang, M. Prehm, X.H. Cheng, C. Tschierske, J. Mater. Chem. C. 3 (2015) 1301.
[22] V. Soghomonian, Q. Chen, R.C. Haushalter, J. Zubieta, C.J. O'Connor, Science 259 (1993) 1596.
[23] (a) M. Peterca, V. Percec, M.R. Imam, P. Leowanawat, K. Morimitsu, P.A. Heiney, J. Am. Chem. Soc. 130 (2008) 14840;
(b) W.L. Sun, S.B. Li, H.Y. Ma, H.J. Pang, L. Zhang, Z.F. Zhang, RSC Adv. 4 (2014) 24755.
[24] (a) L. Han, H. Valle, X.H. Bu, Inorg. Chem. 46 (2007) 1511;
(b) B. Ding, Y.Y. Liu, X.X. Wu, X.J. Zhao, G.X. Du, E.C. Yang, X.G. Wang, Cryst. Growth Des. 9 (2009) 4176.
[25] C.R. Deltcheff, M. Fournier, R. Franck, R. Thouvenot, Inorg. Chem. 22 (1983) 207.
[26] (a) G.M. Sheldrick, SHELX-97, Program for Crystal Structure Refinement, University of Göttingen, Germany, 1997;
(b) G.M. Sheldrick, SHELXL-97, Program for Crystal Structure Solution, University of Göttingen, Germany, 1997.
[27] I.D. Brown, D. Altermatt, Acta Crystallogr., Sect. B: Struct. Sci. 41 (1985) 244.
[28] A.I. Vogel, Textbook of Practical Organic Chemistry, Longman Group Limited, London, 1978.
[29] L. Pizzio, P. Vazquer, Catal. Lett. 77 (2001) 233.